This article has been accepted for publication in a future issue of this journal, but has not been fully edited. Content may change prior to final publication. Citation information: DOI 10.1109/TCAD.2019.2942002, IEEE Transactions on Computer-Aided Design of Integrated Circuits and Systems

Multi-Target Sample Preparation Using MEDA Biochips

Tung-Che Liang, Yun-Sheng Chan, Tsung-Yi Ho, *Senior Member, IEEE*, Krishnendu Chakrabarty, *Fellow, IEEE*, Chen-Yi Lee

***Abstract*—Sample preparation, as a key procedure in many biochemical protocols, mixes various samples and/or reagents into solutions that contain the target concentrations. Digital microfluidic biochips (DMFBs) have been adopted as a platform for sample preparation because they provide automatic procedures that require less reactant consumption and reduce human-induced errors. However, most existing methods only consider two-reactant sample preparation, and they cannot be used for many biochemical applications that involve multiple reactants. In addition, existing methods that can be used for multiple-reactant sample preparation were proposed on traditional DMFBs where only the (1:1) mixing model is available. In the (1:1) mixing model, only two droplets of the same volume can be mixed at a time, which results in higher completion time and the wastage of valuable reactants. To overcome this limitation, the micro-electrode-dot-array (MEDA) architecture has been introduced; it provides the flexibility of mixing multiple droplets of different volumes in a single operation. In this paper, we present a generic multiple-reactant sample preparation algorithm that exploits the novel fluidic operations on MEDA biochips. We also propose an enhanced algorithm that increases the operation-sharing opportunities when multiple target concentrations are needed, and therefore the usage of reactants can be further reduced. Simulated experiments show that the proposed method outperforms existing methods in terms of saving reactant cost, minimizing the number of operations, and reducing the amount of waste.**

I. Introduction

Sample preparation is an essential step in many biochemical protocols for generating reagents with a range of desired concentrations. For example, in drug design, to determine the minimum inhibitory concentration, various antibiotics are first diluted to different target concentrations, and the diluted antibiotics are tested to arrest the growth of the bacteria [2], [3]. Moreover, it has also been reported that 90% of the cost and 95% of the bioassay execution time in molecular diagnosis are associated with sample preparation [4]. Therefore, it is critical to provide an automated sample-preparation process for numerous bio-chemical applications.

Digital microfluidic biochips (DMFBs) have been adopted as a technology platform for sample preparation [5], [6], [7]. A DMFB manipulates discrete fluid droplets on a two-dimensional electrode array. When driven by a sequence of control voltages, the electrode array can perform fluidic operations such as dispensing, mixing, and splitting [8], [9]. By serially performing mixing and splitting on loaded samples, automated sample preparation can be carried out on the DMFBs. Because these operations can be pre-programmed in the control unit of the DMFBs, the overall procedure is efficient and less prone to human-induced errors.

Several sample preparation algorithms have been proposed to automate the overall process using DMFBs [10], [11]. However, most existing methods only consider one case of sample preparation that involves only two reactants, and this type of sample preparation cannot be used in many real-life applications that require more than two reactants. For example, the polymerase chain reaction (PCR) is widely used as a biological tool for amplifying specific gene segments in a DNA sample. The "buffer" solution that is used in PCR provides a critical environment with various compounds such as Tris-HCl, KCl, and $MgCl_2$ [12]. These compounds need to be mixed to a specific concentration according to the characteristics of the gene in a DNA segment before PCR is carried out. Likewise, multiple-reactant sample preparation is also used to mix multiple compounds for other biochemical applications, including drug discovery and drug delivery [13], [14], [15].

Even though a few existing algorithms can be used for multiple-reactant sample preparation on DMFBs [10], [16], [17], [18], [19], these methods suffer from the limitation that only one specific mixing operation can be carried out on DMFBs. For example, the common-dilution-operation-sharing (CoDOS) algorithm explores sharing opportunities using a recipe matrix for multiple-reactant bioassays [16]. However, these algorithms are implemented on conventional DMFBs that only provide a (1:1) mixing model. The (1:1) mixing model can only combine two same-size droplets and then split the merged droplet into two resultant droplets after mixing. Thus, if the desired concentration is composed of numerous reactants, many operations are required to mix every reactant until the desired concentration is achieved. To produce a unit-volume droplet with a concentration value of $\langle 9, 5, 2\rangle$ (which specifies the corresponding volume of three reactants), CoDOS requires a total of four mixing operations and generates four units of waste droplets. This lengthy procedure results in the consumption of many reagent droplets and requires a long time, which diminishes the benefits of applying sample preparation on DMFBs.

For biochemical applications that require multiple-reactant sample preparation, there is a need to generate many target

A preliminary version of this paper appeared in the Proceedings of ACM Asia and South Pacific Design Automation Conference (ASP-DAC) [1], 2019.

Tung-Che Liang and Krishnendu Chakrabarty are with the Department of Electrical and Computer Engineering, Duke University, Durham, NC 27708, USA (email: tung.che.liang@duke.edu; krish@duke.edu).

Yun-Sheng Chan and Chen-Yi Lee are with the Department of Electronics Engineering, National Chiao Tung University, Hsinchu 30010, Taiwan (email: yschan@si2lab.org; cylee@si2lab.org).

Tsung-Yi Ho is with the Department of Computer Science, National Tsing Hua University, Hsinchu 30013, Taiwan (e-mail: tyho@cs.nthu.edu.tw).

The work of Tung-Che Liang and Krishnendu Chakrabarty was supported in part by the US National Science Foundation under grant no. 1702596 and grant no. 1914796.

concentrations in order to optimize bioassays. For example, in PCR, appropriate parameter settings are needed for the temperatures of the thermal cycles as well as the reagent concentrations [20], [21]. However, a given parameter setting may only be feasible on certain DNA segments because the success in PCR is influenced by a myriad of factors including the nucleobase sequence, the base-pair lengths of DNA templates, thermal cycle temperatures and the ratio between DNA templates and primers [22], [23], [24]. When one parameter setting is not feasible on a given DNA segment, a new parameter setting which contains different concentration values or varied thermal temperatures should be tested for the DNA sample again. Therefore, to optimize the PCR protocol for distinct DNA samples, molecular and gene scientists need to generate many required solutions in a gradient of concentrations. Similarly, multiple-target sample preparation is also needed in drug discovery using microfluidics [25], [26].

A next-generation DMFB has been proposed based on the micro-electrode-dot-array (MEDA) architecture [27], [28]. MEDA biochips consist of a large number of micro-electrodes, and the microelectrodes can be dynamically grouped to act as actuators for various new types of droplet operations such as dispensing different sizes of droplets and lamination mixing [27]. Based on these novel operations, a mixing operation that blends more than two droplets of different sizes can be achieved on MEDA biochips. With this mixing operation, the MEDA biochip serves as a more suitable platform than the traditional DMFB for multiple-reactant sample preparation. In addition, MEDA biochips offer real-time sensing that can be used as feedback to ensure bioassay execution [28], [29].

In this paper, we present the first multiple-reactant sample-preparation method for MEDA biochips. The proposed method utilizes a generalized mixing model that can blend multiple droplets in a single operation. The key contributions of this paper are as follows:

1) We review novel MEDA-enabled operations and present a generalized mixing model. This mixing model generalizes the mixing of several droplets in different volumes and concentrations in one operation.

2) We present a multiple-reactant sample-preparation approach for MEDA biochips, named *multiple-reactant cost minimization* (MRCM). It utilizes integer linear programming to find an optimal mixing solution based on the given cost of each reactant.

3) We propose an enhanced MRCM, called *e-MRCM*, that can explore the sharing operations between dilution processes for target concentrations in order to reduce the reactant cost, time consumption and waste production.

4) We showcase the effectiveness of the proposed method by comparing it with existing algorithms using simulated experiments. The experimental results reveal that the proposed method can effectively reduce the cost of reactant usage, the number of mixing steps, and the amount of waste.

The remainder of this paper is organized as follows. Section II describes previous work on sample preparation. Section III explains sample preparation on MEDA biochips and presents the problem formulation. Section IV elaborates the details of the proposed sample-preparation algorithm. Section V details the enhanced MRCM that exploits the sharing operations between dilution processes and generates lower-cost dilution processes for multi-target sample preparation. Section VI presents experimental results. Finally, conclusions are drawn in Section VII.

II. Background

In this section, we first introduce mixing models that are used in sample preparation. We next introduce the use of a directed graph to illustrate the sample-preparation process. Finally, we describe previous sample-preparation algorithms.

A. Mixing Models and Sample Preparation

Previous work on DMFBs typically adopts (1:1) mixing operations, which mix two droplets with the same volume size, to dilute reagents and samples into specific concentration values. The concentration value of a resultant droplet r after a (1:1) mixing operation can be calculated as

$$CV_r = \frac{CV_1 + CV_2}{2} \tag{1}$$

where CV_1 and CV_2 represent the concentration values of the two source droplets before mixing, respectively.

Previous work on *flow-based microfluidic biochips* (FMFBs), on the other hand, exploits the use of a rotary mixer that can blend more-than-two solutions in a single mixing operation [30], [31]. A rotary mixer contains N independent segments, and each segment can be filled with a fluid with a distinct concentration value. Therefore, a general mixing model $(s_1 : s_2 : ... : s_M)$ can be used for sample preparation, where M is the number of fluids that are mixed, and s_i represents the respective volume size of fluid i. The concentration value of a resultant droplet r after the general mixing model can thus be calculated as

$$CV_r = \frac{\sum_{i=1}^{M} s_i \times CV_i}{\sum_{i=1}^{M} s_i} \tag{2}$$

where CV_i represents the concentration value of source fluid i before mixing. MEDA biochips also provide mixing operations that can blend more than two droplets; these operations will be introduced in Section III-A. Using these operations, prior work on sample preparation has also considered the general mixing model [1], [32], [33].

B. Dilution Graph

The sample-preparation process can be illustrated as a directed graph, referred to as a *dilution graph* or a *dilution tree* [11], [16], [34]. Nodes with in-degree zero represent original reactant droplets, and the node with out-degree zero stands for the output droplet with the target concentration. Each node in the dilution graph is labeled with its concentration value; edges represent volume flow from one droplet to another. Nodes in the dilution graph are double circled if they are not fully utilized. Examples of dilution graphs are provided in Fig. 1.

C. Previous Work

Several approaches, such as BS [10] and REMIA [11], were proposed to solve the two-reactant sample preparation. For the two-reactant sample preparation, a valuable sample/reagent is diluted to a specific concentration value using a buffer solution.

This article has been accepted for publication in a future issue of this journal, but has not been fully edited. Content may change prior to final publication. Citation information: DOI 10.1109/TCAD.2019.2942002, IEEE Transactions on Computer-Aided Design of Integrated Circuits and Systems

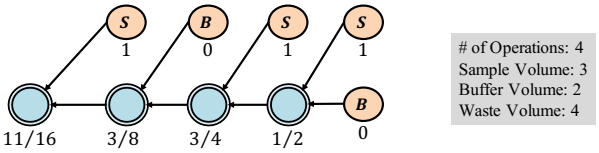

(a) The dilution process using the BS method.

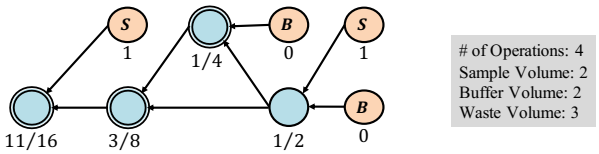

(b) The dilution process using the REMIA method.

Fig. 1: Dilution graphs for a target concentration $\frac{11}{16}$ using (1:1) mixing operations on traditional DMFBs. Double-circled nodes are not fully utilized.

The BS approach first transforms a target concentration CV into a binary representation and performs the dilution process based on this binary representation, where $0 \leq CV \leq 1$. A bit '1' in the representation indicates that a sample droplet should be used for a mixing operation; whereas, a bit '0' in the representation signals the use of a buffer droplet for another mixing operation. For example, if BS is given a target concentration $CV = \frac{11}{16} = 0.1011_2$, the dilution process follows the binary representation from the least significant bit (LSB) to the most significant bit (MSB) as shown in Fig. 1(a). Because each bit is related to a mixing operation with either the sample or the buffer, the length of the binary representation determines the total number of mixing operations. An inherent feature of the BS approach is that only one droplet is kept after the mixing operation while the other droplet is discarded as waste. Therefore, the consumption of samples and the production of waste are increased. On the other hand, the REMIA approach assumes that the sample/reagent is precious and minimizes its use. REMIA first generates a skewed mixing tree, which contains leaf nodes with *prime concentration values* [11]. The prime concentration values are exponential concentration values obtained by serial (1:1) dilution. REMIA then produces the leaf nodes with the minimum usage of the valuable reactant. An example of the sample preparation process using REMIA is shown in Fig. 1(b). In this case, the nodes with concentration values $\frac{1}{4}$ and $\frac{1}{2}$ are the prime concentration values that can be diluted using only one sample droplet. Thus, for the same target concentration value, REMIA consumes less reagent usage compared to BS. Although REMIA requires less reagent usage compared to BS, REMIA cannot be used for multiple-reactant sample preparation, which is common in many biochemical applications. Note that for both cases, we assume that the volume of the required droplet is one unit. However, after the last (1:1) mixing operation, a two-unit-volume droplet of the target concentration is produced. Therefore, after splitting, only one droplet is used and the other is regarded as waste.

To process multiple-reactant sample preparation on DMFBs, CoDOS [16] was introduced using a recipe matrix. CoDOS uses a concentration vector $\mathbf{CV}$ to specify corresponding volumes of various reactants in a droplet. (Note that the notation for the concentration vector $\mathbf{CV}$ differs from that of the concentration value CV for two-reactant sample preparation.) CoDOS then represents the target concentration, $\mathbf{CV}$, into a recipe matrix. For example, if $\mathbf{CV} = \langle 5, 7, 4 \rangle$, the translated recipe matrix is shown in Fig. 2(a). The '1's in the recipe matrix indicate the respective reactant usage in the sample-preparation process. By looking at the column 2^{-4}, we learn that droplets of reactant 1 and reactant 2 need to be dispensed and mixed first, and then the mixed droplet should be merged with another droplet of reactant 2 in column 2^{-3}. Let the concentration vector of reactant 1 be $\mathbf{CV}(\mathbf{1})$ and the concentration vector of reactant 2 be $\mathbf{CV}(\mathbf{2})$, where $\mathbf{CV}(\mathbf{1}) = \langle 16, 0, 0 \rangle$ and $\mathbf{CV}(\mathbf{2}) = \langle 0, 16, 0 \rangle$. The concentration vector of the resultant droplet r can be calculated using Equation (1): $\mathbf{CV}(\mathbf{r}) = \frac{\mathbf{CV(1)}+\mathbf{CV(2)}}{2} = \langle 8, 8, 0 \rangle$. The corresponding dilution tree is shown in Fig. 2(a). Because there are three '1's in the 2^{-2} column and we can only use the (1:1) mixing operation, there are $\binom{3}{2}$ ways of mixing two of them together in the corresponding level. With the use of the recipe matrix, we can easily identify the sharable mixing operation within a dilution tree (circled in red in Fig. 2(a)). If we mix droplets of reactant 1 and reactant 2 at the 2^{-2} level, this operation can be shared with the mixing operation at level 2^{-4}. Therefore, we can save the usage of valuable reactants and reduce the waste production; see Fig. 2(b). However, the sharing opportunity may decrease when the number of reactants increases, i.e., the number of rows increases in the recipe matrix. When there is no sharing opportunity within the dilution tree, the reactant saving is insignificant. In addition, the automated procedure may become inefficient because of the many required mixing operations.

In contrast to sample preparation methods on traditional DMFBs, WSPM [34] was proposed for MEDA biochips. This method adopts MEDA-enabled fluidic operations and uses a general mixing model (m:n), where neither m nor n need to be 1, to achieve the target concentration. The use of the general mixing model (m:n) can significantly reduce the number of dilution steps compared to the (1:1) mixing operation on DMFBs. An example is illustrated in Fig. 3. To generate a droplet with $CV = \frac{21}{64}$, REMIA requires a total of six mixing operations and two volume of the sample. The dilution graph is shown in Fig. 3(a). However, WSPM needs only one mixing operation and one unit volume of the sample because it exploits the (1:2) mixing model. The associated dilution graph is shown in Fig. 3(b). Note that WSPM generates the target concentration $CV = \frac{21}{64}$ using the approximation of $CV = \frac{1}{3}$ with an acceptable accuracy error e, where $e < \frac{0.5}{64}$. The experimental experiments in [34] also show that WSPM requires fewer mixing operations than the previous methods. However, similar to REMIA, WSPM cannot be applied to multiple-reactant sample preparation, which is necessary in many biochemical applications.

III. Sample Preparation on MEDA

In this section, we introduce MEDA-enabled operations that support a general mixing model that can mix multiple reactants. We also demonstrate operations on fabricated MEDA

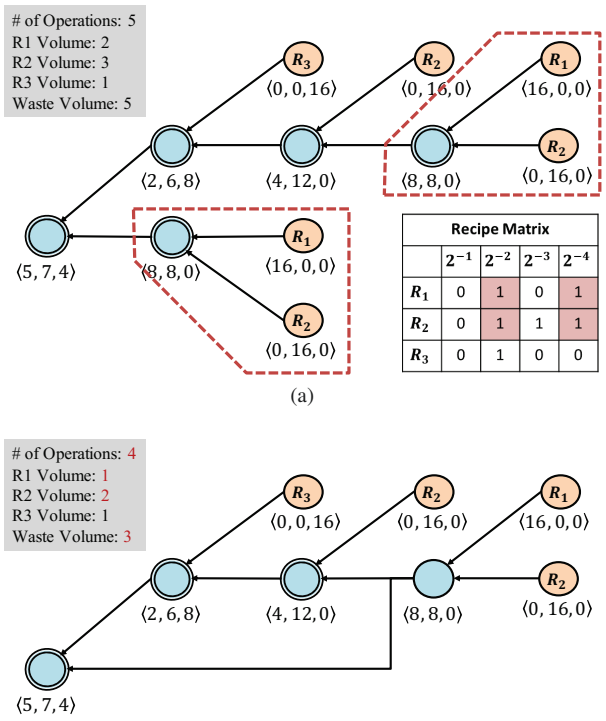

Fig. 2: Dilution graphs for $\mathbf{CV} = \langle 7, 5, 4 \rangle$ using the (1:1) mixing operations on traditional DMFBs. (a) The recipe matrix indicates the sharable mixing operation at level 2^{-2} and 2^{-4}. (B) The dilution graph after operation sharing.

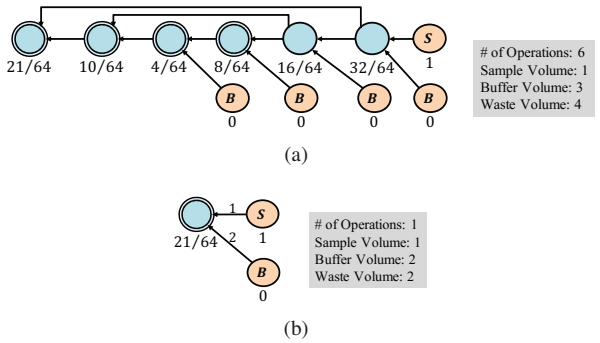

Fig. 3: Dilution graphs generated by (a) REMIA, and (b) WSPM.

biochips in our laboratory. The biochips were fabricated at TSMC using a $0.35\,\mu\text{m}$ process [35]. We then describe the concept of a dilution graph for the multiple-reactant-sample-preparation process. Finally, the multiple-reactant sample-preparation problem is formally described.

A. New Operations on MEDA Biochips

Recall that micro-electrodes on MEDA biochips are dynamically grouped to form various actuators, and the actuators provide diverse fluidic operations [36], [37]. One such operation is *channel dispensing* [27], shown in Fig. 4. Unlike splitting on conventional DMFBs, channel dispensing on MEDA biochips controls the sizes of the two resultant droplets in a fine-grained manner. The steps in channel dispensing are as follows: 1) The original droplet is actuated to form a channel that flows toward to the micro-electrodes, where the new droplet will be generated. 2) The new droplet is derived from the channel. 3) When the new droplet is grown to the desired volume, the channel breaks in the middle. This procedure can be applied to the same droplet several times. For example, assume a droplet contains a volume of 4X. This droplet can first dispense a 1X volume droplet, and then dispense another 1X volume droplet. As a result, three droplets with volumes of 1X, 1X, and 2X are generated from the original 4X droplet. A similar dispensing method, which is referred to as pseudo dispensing in [34], has also been demonstrated on MEDA biochips.

Likewise, MEDA biochips provide a new type of fluid-merging operation. Since micro-electrodes are dynamically grouped as actuators, various sizes of droplets can be transported on MEDA biochips. Therefore, two different sizes of droplets can be merged into one, e.g., a 1X droplet and a 2X droplet can be merged into a 3X droplet. Fig. 5 shows two droplets with different sizes are merged into one droplet. In addition, more than two droplets can be continuously merged into one. Although the merged droplet might be bigger than a normal-size droplet, the reactants in the droplet can still be mixed thoroughly using a lamination mixer [27]. In *lamination mixing* (see Fig. 6), a droplet is split and recombined repeatedly, and the split direction is perpendicular to the recombine direction. This increases the contact surfaces of the two droplets, and therefore the mixing procedure is accelerated. In contrast to using the electrode-array mixer on DMFBs [8], lamination mixing requires less micro-electrodes on MEDA biochips and thus makes more on-chip area for other concurrent operations.

B. Notation for Multiple-Reactant Sample Preparation

Since a droplet d may consist of N reactants, the concentration value of d can be denoted as $\mathbf{CV(d)}$, which is a vector of length N that specifies the corresponding volume of each reactant. The target concentration is expressed as

$$\mathbf{CV(d)} = \langle v_1^d, v_2^d, ..., v_N^d \rangle \tag{3}$$

where component v_i^d indicates the volume of reactant i in droplet d. The components in the vector are calculated according to the given precision level P.

$$\sum \mathbf{CV(d)} = \sum_{i=1}^{N} v_i^d = \frac{1}{P} \tag{4}$$

For example, if a droplet consists of four different reactants in equal amounts and the precision level $P = 0.001$, the concentration vector equals to $\langle 250, 250, 250, 250 \rangle$.

For a general mixing model $(s_1 : s_2 : ... : s_M)$, let the concentration of each input droplet be denoted as $\mathbf{CV(1)}, \mathbf{CV(2)}, ..., \mathbf{CV(M)}$, and the volume of each droplet d be s_d. The resultant droplet r satisfies the following relationships:

$$\frac{\mathbf{CV(r)}}{\sum(\mathbf{CV(r)})} = \langle \frac{\sum_{i=1}^{M} (\frac{v_1^i}{\sum_{j=1}^{N} v_j^i} \times s_i)}{\sum_{i=1}^{M} s_i}, ..., \frac{\sum_{i=1}^{M} (\frac{v_N^i}{\sum_{j=1}^{N} v_j^i} \times s_i)}{\sum_{i=1}^{M} s_i} \rangle \tag{5}$$

$$s_r \leq \sum_{i=1}^{M} s_i, \text{ where } s_r \in \mathbb{N}^+ \tag{6}$$

This article has been accepted for publication in a future issue of this journal, but has not been fully edited. Content may change prior to final publication. Citation information: DOI 10.1109/TCAD.2019.2942002, IEEE Transactions on Computer-Aided Design of Integrated Circuits and Systems

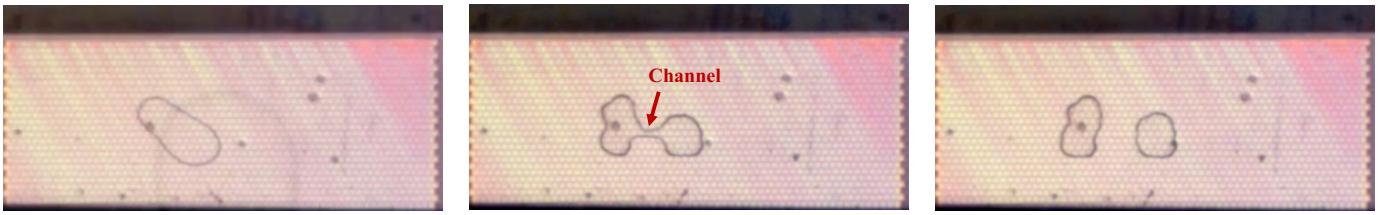

(a) Step 1. (b) Step 2. (c) Step 3.

Fig. 4: Two different sizes of droplets are generated by channel dispensing using a fabricated MEDA biochip in our laboratory. (a) A droplet is forming a channel toward to the left. (b) A new droplet is derived from the channel. (c) The channel breaks in the middle, and two resultant droplets are generated.

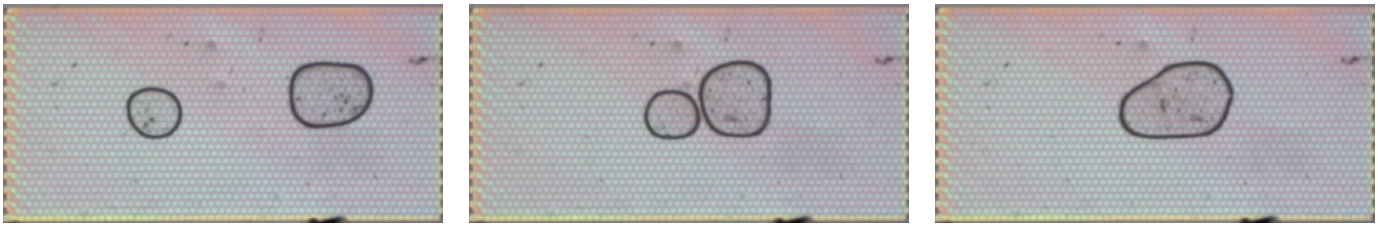

(a) (b) (c)

Fig. 5: Two droplets with different sizes are merged into one droplet using a fabricated MEDA biochip in our laboratory. (a) Two droplets exist on the biochip and the droplet on the left is smaller than the droplet on the right. (b) Two droplets are transported toward the same area on the biochip. (c) The two droplets are merged into a droplet.

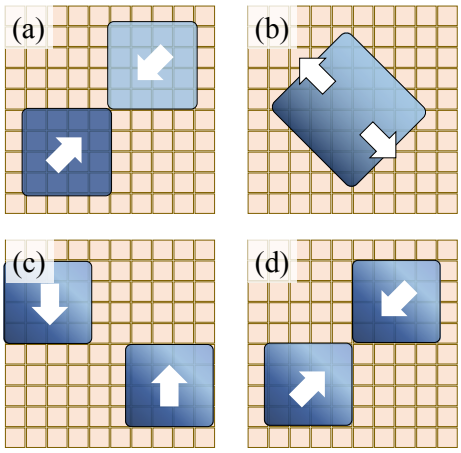

Fig. 6: The steps associated with lamination mixing. (a) Two droplets are merged. (b) The merged droplet is split in the direction that is orthogonal to the merged direction. (c) Two split droplets are transported to the start positions respectively. (d) The same operations are repeated until the droplet is mixed completely.

Equation (5) describes the concentration of the resultant droplet from the general mixing model. Inequality (6) states the volume constraint on droplet mixing, i.e., the volume of the mixed droplet may be larger than the droplet required for the next stage. Besides, experiments have shown that there is a minimum volume constraint associated with the droplets on MEDA biochips, and the minimum-sized aliquot droplet is determined by the size of the MEDA microelectrode [38], [39]. Therefore, the volume of the resultant droplet should be integer multiples of the volume of the aliquot droplet.

C. Comparison Between DMFBs and MEDA Biochips in Terms of Mixing Operations

With the use of mixing operations with various mixing ratios on MEDA biochips, the dilution process can be expedited. For example, suppose a target concentration $\mathbf{CV(r)} = \langle 1, 2 \rangle$ is given, and we aim to generate a droplet with this concentration on a traditional 2D DMFB and on a MEDA biochip, respectively. For the DMFB, which only offers the (1:1) mixing operation, the fastest way is to have three successive mixing operations using the BS approach. The process of sample preparation is shown in Fig. 7(a). However, on the MEDA biochip, the target concentration can be easily achieved using a $(1:2)$ mixing operation; see Fig. 7(b).

The above example illustrates the case when the target concentration contains only two reactants. When the target concentration contains N reactants ($N > 2$), the minimum number of operations OP_{min} using only the $(1:1)$ mixing model can be expressed as $OP_{min} \geq N - 1$ because each mixing operation can only take a maximum of two original reactants. The best-case scenario is that all original reactants are mixed by operations that take two of them at a time. Based on this observation, the more reactants that a target concentration contains, the more mixing operations are needed for the dilution process. Note that the observation reveals a lower bound on the number of mixing operations when the (1:1) mixing model is used. As mentioned in Section II, many sample-preparation methods have been proposed in the past few years [10], [11], [16], and one of the optimization goals in these methods is to reduce the number of mixing operations. The fewer mixing operations, the less time it takes to prepare the target mixture. As a result, an upper bound on the number

This article has been accepted for publication in a future issue of this journal, but has not been fully edited. Content may change prior to final publication. Citation information: DOI 10.1109/TCAD.2019.2942002, IEEE Transactions on Computer-Aided Design of Integrated Circuits and Systems

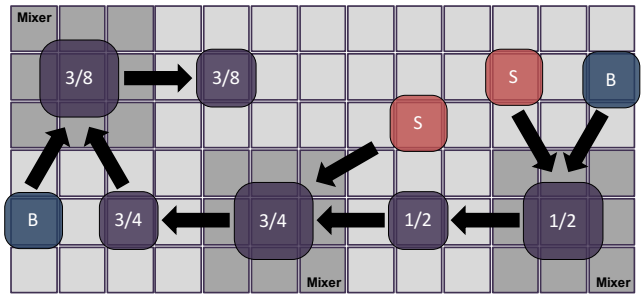

(a)

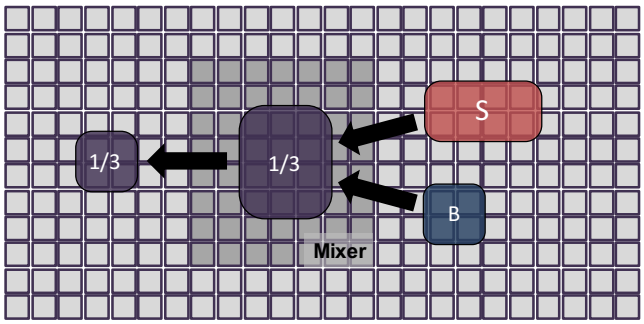

(b)

Fig. 7: Comparison between two platforms for acquiring a droplet with concentration value $CV = \frac{1}{3}$. (a) Three (1:1) mixing operations are required on a DMFB. (b) Only one mixing operation (1:2) is needed to achieve concentration $CV = \frac{1}{3}$ on a MEDA biochip.

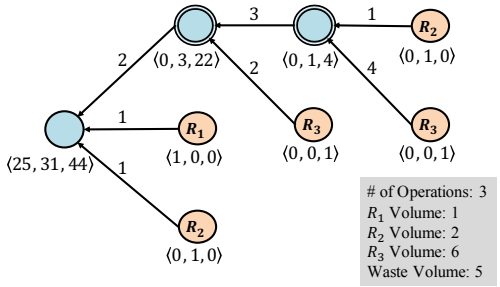

(a)

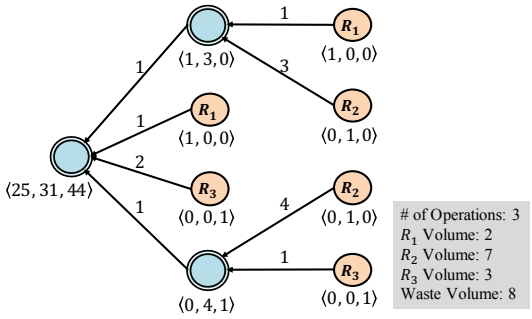

(b)

Fig. 8: Dilution graphs for a target droplet with the concentration $\langle 25, 31, 44\rangle$ and the size 4X using the general mixing model on MEDA biochips. (a) The best dilution tree when R_1 is the most valuable reactant among all. (b) The best dilution tree when R_3 is the most valuable reactant among all.

of mixing operations is not as much of a concern, and it tends to be a loose bound. Another drawback of using only the (1:1) mixing model is that only concentrations that are expressed as a power of 2 can be generated without errors. In the example of Fig. 7, $CV = \frac{1}{3}$ cannot be generated on traditional 2D DMFBs, so a concentration value of $\frac{3}{8}$ is produced instead with an error of $\frac{3}{8} - \frac{1}{3} = \frac{1}{24}$. However, on MEDA platforms, the desired concentration can be achieved without this inherent error.

D. Dilution Graph

Like the previous sample preparation methods described in Section II, we also use a dilution graph to illustrate the multiple-reactant-sample-preparation process. However, considering the mixing multiple reactants using the proposed general mixing model, we explicitly label the volume flow from one droplet to another on the edges, and the volume corresponding to a node is determined by the sum of its input edges.

An example of a dilution graph is provided in Fig. 8(a). The target is a 4X droplet with a concentration of $\langle 25, 31, 44\rangle$, and the precision level $P = \frac{1}{25+31+44} = \frac{1}{100}$. The type of the mixing model is represented by the node with its input edges. For instance, the output node with the target concentration is generated by a (2:1:1) mixing model, and its input edges are labeled with 2, 1, and 1, respectively. The concentration of the output droplet $\mathbf{CV}(\mathbf{r})$ can be calculated based on the mixing model using Equation (5):

$$\frac{\mathbf{CV}(\mathbf{r})}{\sum(\mathbf{CV}(\mathbf{r}))} = \langle \frac{\sum_{i=1}^{M}(\frac{v_1^i}{\sum_{j=1}^{N} v_j^i} \times s_i)}{\sum_{i=1}^{M} s_i}, ..., \frac{\sum_{i=1}^{M}(\frac{v_N^i}{\sum_{j=1}^{N} v_j^i} \times s_i)}{\sum_{i=1}^{M} s_i} \rangle$$
$$= \langle \frac{0+1+0}{2+1+1}, \frac{2\times\frac{3}{25}+0+1}{2+1+1}, \frac{2\times\frac{22}{25}+0+0}{2+1+1} \rangle$$
$$= \frac{\langle 25, 31, 44\rangle}{100}$$

In a mixing operation, waste fluids are produced when the input volume is higher than the required volume for the next stage. For example, the node with the concentration of $\langle 0, 1, 4\rangle$ in Fig. 8(a) is mixed with a total of 5X droplets, but the requirement for the next mixing operation of this droplet is only 3X. As a result, the mixed 5X droplet is split into a 3X droplet and a 2X droplet, and the 2X droplet is discarded as a waste. Nodes in the dilution graph are double circled if they are not fully utilized.

E. Problem Formulation

To achieve the optimization goal of reducing sample/reagent usage in sample preparation, the cost of each reactant needs to be considered. The valuable reactants or expensive reagents usually determine the cost of the overall procedure. However, the corresponding values of the required reactants can only be determined when the bioassay is being executed, i.e., the value of each reactant is determined according to the execution circumstance. For example, the cost of an infant's blood is generally higher than the cost of the same volume blood from an adult; for the same clinical diagnosis, we would like to reduce the usage of blood sample in the infant's case, and we

This article has been accepted for publication in a future issue of this journal, but has not been fully edited. Content may change prior to final publication. Citation information: DOI 10.1109/TCAD.2019.2942002, IEEE Transactions on Computer-Aided Design of Integrated Circuits and Systems

TABLE I: Notation used to describe MRCM.

Symbol	Description
N	Number of reactants
M	Number of source droplets in a mixing model
$\mathbf{CV(r)}$	Concentration vector of droplet r
$\mathbf{CV(r)}^T$	Vector transpose of $\mathbf{CV(r)}$
$(s_1\text{: } s_2\text{:...:}s_M)$	A mixing model that blends M droplets, where s_i represents the volume of the i^{th} source droplet
$\mathbf{C_{M,N}}$	A concentration matrix that contains concentration vectors for source droplets in a mixing model

may aim to reduce another valuable reagent in the adult's case. Therefore, the cost of each reactant should be evaluated in the multiple-reactant sample preparation.

Recall that for many bioassays, sample preparation is the first essential step to prepare droplets in specific concentrations and volumes. The prepared droplets are then used for the following procedures in bioassays. Because MEDA biochips can manipulate droplets with different volumes, the volume of the target droplet should be carefully considered during sample preparation.

The problem of the multiple-reactant sample preparation is formally stated as follows:
Inputs: (1) target concentration vector $\mathbf{CV}$, (2) size of the target droplet, and (3) the cost of each reactant $\mathbf{W} = \langle w_i \rangle$.
Output: A mixing process, which is presented by a dilution graph, that produces the target droplet using the general mixing model.
Objective: Minimize the overall cost of reactants by considering the weight of each reactant, the needs of the mixing operations, as well as the waste production.

IV. Proposed Algorithm

In this section, we first present a search method that generates all possible mixing opportunities when given a droplet with the concentration and the volume size. In table I, we also list notation used in this section. A *multiple-reactant cost minimization* (MRCM) algorithm for sample preparation is then presented. MRCM consists of two stages. In the first stage, it exploits the search method from the target concentration and explores all possible dilution trees. In the second stage, the algorithm selects the best dilution tree using the given reactant costs.

A. ILP-Based Mixing Exploration

Although the general mixing model in Section III does not specifically constrain the size of lamination mixers on MEDA biochips, we define a limit for the size of a mixing model for MRCM due to practical reasons. To avoid occupying a large area for a mixing operation, we assume (without loss of generality) that the maximum size of the mixer is 8 times bigger than the minimum droplet on MEDA biochips. That is, when the size of the minimum droplet is m, the multiple-mixing model $(s_1 : s_2 : ... : s_M)$ must obey the following equation.

$$\sum_{i=1}^{M} s_i \leq 8m,\ m \in \mathbb{N} \tag{7}$$

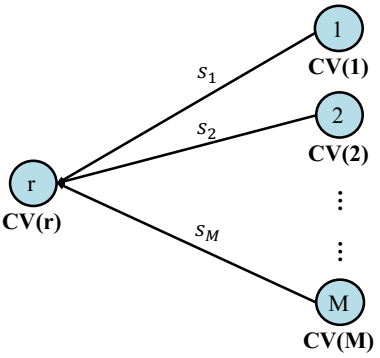

Fig. 9: The generalized multiple-reactant mixing model. M droplets are mixed in the ratio $(s_1 : s_2 : ... : s_M)$ to a resultant droplet r.

Therefore, when $m = 1$, the (1:3) and (2:2:2:2) mixing models are all legal, but the (4:5) mixing model is not admissible. All mixing models that follow Equation (7) can be enumerated using the integer partitioning method [40]. For example, 4 can be obtained as $1+3$, $2+2$, $1+1+2$, or $1+1+1+1$. Therefore, for mixing models that $\sum_{i=1}^{M} s_i = 4$, (1:3), (2:2), (1:1:2), and (1:1:1:1) are the legal mixing models. All legal mixing models are enumerated first using the integer partitioning method, and these legal models are stored for the following steps in mixing exploration.

When a droplet r is given with the concentration vector $\mathbf{CV(r)}$ and the volume size s_r, we can find all legal mixing opportunities to generate r based on the precomputed legal mixing models. The general mixing model is presented in Fig. 9. Assuming that the droplet r can be mixed by M input droplets, which are denoted as 1 to M, the $\mathbf{CV(r)}$ must follow the concentration relationship in Equation (5), and s_r must obey the volume inequality in Equation (6). As a result, the component v_i^r in $\mathbf{CV(r)}$ can be computed using Equation (8):

$$\frac{v_i^r}{\sum_{i=0}^{N} v_i^r} = \frac{\sum_{j=1}^{M} (s_j \times \frac{v_i^j}{\sum \mathbf{CV(j)}})}{\sum_{j=1}^{M} s_j} \tag{8}$$

Each component v_i^r in $\mathbf{CV(r)}$ shares the same values of $\sum v_i^r$ and $\sum s_j$. To simplify the expression of the resultant concentration, let vector $\mathbf{S} = \langle s_1, s_2, ..., s_M \rangle$ be the mixing volume ratio of the input droplets, and let matrix $\mathbf{C_{M,N}}$ contain concentrations of input droplets, where

$$\mathbf{C_{M,N}} = \begin{bmatrix} \mathbf{CV(1)}^T \\ \mathbf{CV(2)}^T \\ \vdots \\ \mathbf{CV(M)}^T \end{bmatrix} = \begin{bmatrix} v_1^1 & v_2^1 & \cdots & v_N^1 \\ v_1^2 & v_2^2 & \cdots & v_N^2 \\ \vdots & \vdots & \ddots & \vdots \\ v_1^M & v_2^M & \cdots & v_N^M \end{bmatrix} \tag{9}$$

By re-organizing the components in $\mathbf{CV(r)}$ using Equation (8), we can express $\mathbf{CV(r)}$ as:

$$\frac{\sum(\mathbf{S}) \times \prod_{i=1}^{M} \sum(\mathbf{CV(i)})}{\sum(\mathbf{CV(r)})} \mathbf{CV(r)} = \mathbf{C_{M,N}}^T \cdot \mathbf{S} \tag{10}$$

When we are given $\mathbf{CV(r)}$, s_r, and a mixing model ratio $\mathbf{S} = \langle s_1, s_2, ..., s_M \rangle$, we can seek an optimal solution under

This article has been accepted for publication in a future issue of this journal, but has not been fully edited. Content may change prior to final publication. Citation information: DOI 10.1109/TCAD.2019.2942002, IEEE Transactions on Computer-Aided Design of Integrated Circuits and Systems

Equations (6), (7), and (10) using integer linear programming (ILP). The search method aims to generate child nodes that are original reactants or that can be generated by original reactants. Therefore, the minimization goal for ILP is to generate the child nodes with the smallest sum of its concentration vector, i.e., minimizing $\sum_i \sum_j v_i^j$. Since the mixing model ratios are known and finite, all possible mixing solutions for the target droplet can be exhaustively found. Therefore, the ILP-based mixing exploration can be formally described below:

Minimize:

$$\sum_i \sum_j v_i^v$$

Subject to:

Volume constraint: $s_r \leq \sum_{i=1}^{M} s_i$, where $s_r \in \mathbb{N}^+$

Mixing model constraint: $\sum_{i=1}^{M} s_i \leq 8m$, $m \in \mathbb{N}$

Concentration equality:

$$\frac{\sum(\mathbf{S}) \times \prod_{i=1}^{M} \sum(\mathbf{CV(i)})}{\sum(\mathbf{CV(r)})} \mathbf{CV(r)} = \mathbf{C_{M,N}}^T \cdot \mathbf{S}$$

For example, let $\mathbf{CV(r)} = \langle 25, 31, 44 \rangle$ and $s_r = 4$, which is the example in Fig. 8. A solution can be found using the ILP-based mixing exploration. A mixing model ratio $\mathbf{S} = \langle 2, 1, 1 \rangle$ is selected from the precomputed legal mixing models according to Equation (6) and Equation (7). Based on the mixing model selection, we know that $M = 3$ and $N = 3$. As a result, there are a total of nine variables in the concentration matrix $C_{3,3}$. According to the minimization goal and Equation (10), an optimal solution can be found as $\mathbf{CV(1)} = \langle 0, 3, 22 \rangle$, $\mathbf{CV(2)} = \langle 1, 0, 0 \rangle$, and $\mathbf{CV(3)} = \langle 0, 1, 0 \rangle$. Similarly, another legal mixing model ratio $\mathbf{S} = \langle 1, 1, 2, 1 \rangle$ is selected from the ILP-based mixing exploration, and another solution can be found as $\mathbf{CV(1)} = \langle 1, 3, 0 \rangle$, $\mathbf{CV(2)} = \langle 1, 0, 0 \rangle$, $\mathbf{CV(3)} = \langle 0, 0, 1 \rangle$, and $\mathbf{CV(4)} = \langle 0, 4, 1 \rangle$.

B. Generation of Dilution Trees

For a given target droplet with the specified concentration and size, the goal is to generate a complete dilution tree, where the root node is the target droplet and the leave nodes are original reactants. The dilution trees can be grown using the search method described in the previous subsection. Therefore, we refer to a complete dilution tree as a *fully-grown tree*; we also define a tree in which leave nodes are not original reactants as a *partially-grown tree*. MRCM first initializes an empty queue GT and an empty list FT, where GT stores the partially-grown trees and FT stores the fully-grown dilution trees. MRCM then sets the target droplet as the root node, and pushes it into GT. Whenever there is a partially-grown tree in GT, MRCM checks if the first tree is fully-grown. If its leave nodes are all original reactants, MRCM stores the tree in FT. Otherwise, MRCM performs the search method to the leave nodes that are not original reactant, and pushes the intermediate (partially grown) back to GT.

C. Selection of the Best Tree

After all possible dilution trees are generated for the given concentration in the previous section, a reactant consumption vector $\mathbf{R}$ is produced for each tree. The component r_i in $\mathbf{R}$ represents the volume consumption of Reactant i, where $1 \leq i \leq N$. The cost of each dilution tree is calculated through the inner product of $\mathbf{R}$ and the given reactant cost vector $\mathbf{W}$, i.e., $\mathbf{R} \cdot \mathbf{W}$. MRCM selects the minimum-cost tree as the solution for the target droplet based on the $\mathbf{R} \cdot \mathbf{W}$ value. An example of various dilution trees for the same target concentration $\langle 25, 31, 44 \rangle$ with size 4X is shown in Fig. 8. For the tree in Fig. 8(a), the associated reactant consumption vector $\mathbf{R_a}$ is produced as $\langle 1, 2, 6 \rangle$; the reactant consumption vector $\mathbf{R_b}$ for the dilution tree in Fig. 8(b) is produced as $\langle 2, 7, 3 \rangle$. If $\mathbf{W} = \langle 1, 1, 1 \rangle$, MRCM will choose the dilution tree in Fig. 8(a) because of the lower reactant cost, i.e., $\mathbf{R_a} \cdot \mathbf{W} < \mathbf{R_b} \cdot \mathbf{W}$. However, if $\mathbf{W} = \langle 2, 1, 3 \rangle$, the overall reactant costs of two trees are 22 and 20, respectively. As a result, MRCM will choose the tree in Fig. 8(b) as the solution because it consumes less reactant cost. If more than two trees share the same cost, MRCM will select the best tree based on the order of the minimum number of mixing operations and then the minimum waste production. The overall flow of MRCM is presented in Fig. 10.

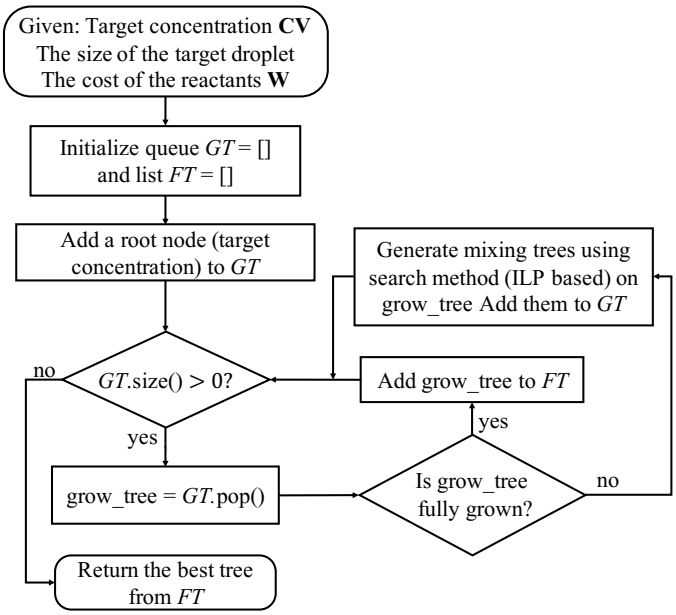

Fig. 10: The overall procedural flow of MRCM.

V. Multiple-Target Sample Preparation

In this section, we first illustrate multiple-target sample preparation to show that further improvement can be made by sharing common operations between dilution trees. We then propose an enhanced MRCM, referred to as e-MRCM, that produces dilution trees with sharable operations.

For example, given a case when two concentration values are needed: $\mathbf{CV(r_1)} = \langle 25, 31, 44 \rangle$ and $\mathbf{CV(r_2)} = \langle 3, 6, 44 \rangle$. The cost of three reactants is also given as $\mathbf{W} = \langle 2, 1, 3 \rangle$. Based on these inputs, MRCM will generate two minimum-cost dilution trees for the two target concentrations, respectively. The minimum-cost dilution trees are shown in Fig. 11(a). However, these two dilution trees do not represent the global optimized solution. Note that according to Section IV,

This article has been accepted for publication in a future issue of this journal, but has not been fully edited. Content may change prior to final publication. Citation information: DOI 10.1109/TCAD.2019.2942002, IEEE Transactions on Computer-Aided Design of Integrated Circuits and Systems

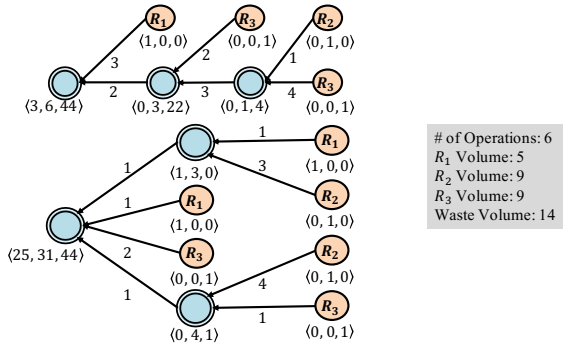

(a) A way of generating $\mathbf{CV(r_1)} = \langle 25, 31, 44\rangle$ with a lower reactant cost.

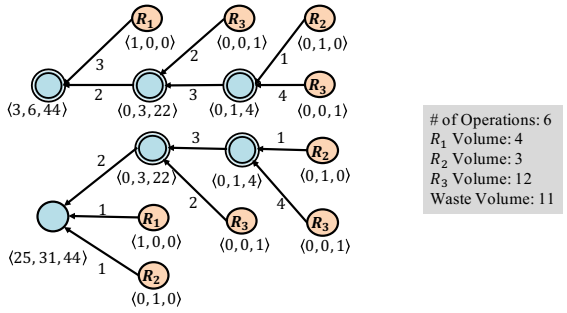

(b) Another way of generating $\mathbf{CV(r_1)} = \langle 25, 31, 44\rangle$ with a higher reactant cost.

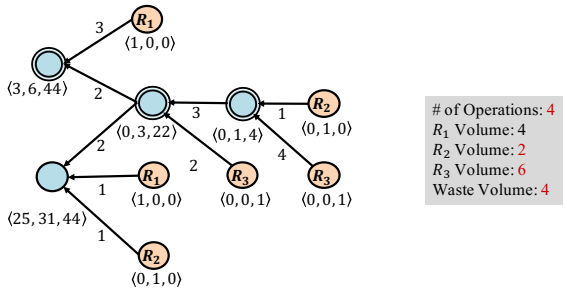

(c) Dilution graph after operation sharing from figure (b). Overall reactant cost is even lower than the process in figure (a)

Fig. 11: Dilution graphs for $\mathbf{CV(r_1)} = \langle 25, 31, 44\rangle$ and $\mathbf{CV(r_2)} = \langle 3, 6, 44\rangle$.

MRCM generates two dilution trees for the target $\mathbf{CV(r_1)} = \langle 25, 31, 44\rangle$ and selects the minimum-cost dilution tree. The two dilution trees for $\mathbf{CV(r_1)}$ are shown in Fig. 11(a) and Fig. 11(b), respectively. In the second phase, MRCM chooses the tree in Fig. 11(a) because of the lower reactant cost. The overall cost of dilution trees in Fig. 11(a) is 46, and the overall cost of dilution trees in Fig. 11(b) is 47. When we compare the overall costs across Fig. 11(a) and Fig. 11(b), it appears that MRCM generates a minimum-cost solution. However, we note that there are some common mixing operations within Fig. 11(b), e.g., nodes with concentration vector $\langle 0, 3, 22\rangle$. Because the resultant droplets from these two operations in the corresponding trees are not fully used, we can share the common operations for the two dilution trees and achieve a lower reactant cost. The dilution graph after operation sharing is shown in Fig. 11(c), and the reactant cost is reduced to 28, which is lower than the result provided by MRCM in Fig. 11(a).

The above example shows that sharing common operations between dilution trees provides better performance in terms of reducing the reactant cost and the number of operations. Even though finding a solution for multiple-target sample preparation is an offline one-time procedure, it is computationally infeasible to obtain an optimal solution using exhaustive search. Note that the time complexity of searching the best sharing opportunity is $O(N^{D\times T})$, where N is the number of nodes in a dilution tree, D is the number of possible dilution trees for a single target, and T is the number of targets. Based on our experiments (presented in Section VI), the average value of N is approximately 6 and the average value of D is approximately 20. For example, for $T = 5$, and the search space to derive an optimal solution includes $6^{20\times 5}$ candidates. To solve the above problem efficiently, e-MRCM adopts two strategies: 1) improving the ILP-based search method (described in Section IV-A) to reduce the search space and 2) generating only dilution trees with sharable nodes.

In MRCM, the ILP-based search method is employed to generate possible parent nodes multiple times when a dilution tree is being grown, and the computation time of the ILP-based search significantly affects the overall performance. Therefore, it is important to speed up the search in order to ensure a better computational performance. Note that if e-MRCM adopts Equation (10) in the ILP search method to explore every possible node, it will generate many dilution trees, and the computation time will increase significantly. Therefore, we reduce the search space by setting the first term in Equation (10) to be 1 and simplifying (10) as

$$\mathbf{CV(r)} = \mathbf{C_{M,N}}^T \cdot \mathbf{S} \tag{11}$$

Equation (8) can also be rewritten as

$$v_i^r = \sum_{j=1}^{M} (s_j \times v_i^j) \tag{12}$$

Equation (12) implies that the component v_i^j in $\mathbf{CV(j)}$ is smaller than the component v_i^r in $\mathbf{CV(r)}$ for all i and j. As a result,

$$\sum(\mathbf{CV(i)}) < \sum(\mathbf{CV(r)}), \text{ for } 1 < i \leq M \tag{13}$$

Our goal in using the search method is to generate parent nodes, original reactants, as fast as possible, i.e., generate nodes i such that $\sum(\mathbf{CV(i)}) = 1$. Equation (13) ensures that the search method will not generate dilution trees where the parent nodes are "larger" than the given child nodes, i.e., $\sum(\mathbf{CV(i)}) > \sum(\mathbf{CV(r)})$, for $1 < i \leq M$.

Without simplifying Equation (10), the ILP-search method is applied to nodes that are not the original reactants in a partially-grown tree. For generating a fully-grown dilution tree for a target concentration, there are P nodes that are not the original reactants within the tree, i.e., the ILP-search method must be used P times. We assume that under the mixing constraint, for each ILP-based search on a node, Q different mixing opportunities are found. Therefore, a total of Q^P dilution trees are generated for a target concentration. With the simplified Equation (11), for each ILP-based search, R different mixing opportunities are found instead, where

This article has been accepted for publication in a future issue of this journal, but has not been fully edited. Content may change prior to final publication. Citation information: DOI 10.1109/TCAD.2019.2942002, IEEE Transactions on Computer-Aided Design of Integrated Circuits and Systems

$R < Q$. As a result, the search space is reduced from Q^P to Q^R.

For the second speed-up strategy, e-MRCM grows dilution trees for all given target concentrations simultaneously and keeps/discards trees with/without sharable common nodes during the tree-generation process. Recall that MRCM stores half-grown dilution trees in a queue named GT and applies the search method on these trees repeatedly until all possible fully-grown trees are generated for a given target concentration. Similarly, given T target concentrations, e-MRCM initializes T queues, named GT_1 to GT_T, to store half-grown dilution trees. Different from MRCM that stores all possible half-grown dilution trees in GT, e-MRCM only keeps the sharable dilution trees in GT_i ($1 \leq i \leq T$). During the dilution-tree generation, e-MRCM keeps recording all non-reactant leave nodes from trees in GT_i and applies the search method first on the node that the sum of its concentration is the largest. After applying the search method on this selected node, the concentration of the selected node is ensured to be larger than that of any newly generated parent node based on Equation (13). In addition, because the sum of the concentration of the selected node is the largest among the non-reactant leave nodes, the newly generated parent node may possibly be shared with other non-reactant leave nodes. When several new dilution trees are generated from the search method, e-MRCM only keeps sharable dilution trees, i.e., e-MRCM discards half-grown dilution trees that cannot be shared, and the effort of growing these non-sharable dilution trees can be avoided.

Based on the above two speed-up strategies, e-MRCM includes the following steps: 1) Given T target concentrations, e-MRCM first initializes T queues, named GT_1 to GT_T, to store partially-grown trees, a sorted list SL, which stores leaf nodes that are non-original-reactant in these growing trees, and a list FT to store fully-grown trees. 2) All target concentrations are added to GT_1 to GT_T as root nodes, respectively. 3) Non-original-reactant leaf nodes in GT_i ($1 \leq i \leq T$) are collected and added to the sorted list SL. Nodes in SL are sorted based on the sum of its corresponding concentration. 4) After SL is updated, a partially-grown tree in GT_i that is related to the largest node in SL is retrieved from GT_i, and e-MRCM applies the search method on this tree. Several possible dilution trees are generated from the search method. If a half-grown tree contains a common node in SL, it will be added back to GT_i; otherwise, all half-grown trees will be added back to GT_i. 5) Whenever GT_i is updated, the corresponding non-original-reactant leaf nodes in GT_i are updated in SL. 6) When a fully-grown tree is generated from GT_i, the corresponding nodes of GT_i in SL are deleted, and the tree is added to FT. The iteration from step 3 to step 6 is repeated until all fully-grown trees are produced for the given target concentrations. The overall flow of e-MRCM is presented in Fig. 12, and the pseudo code of e-MRCM is presented in Fig. 13.

Example: Consider two target concentrations, $\mathbf{CV(r_1)} = \langle 25, 31, 44\rangle$ and $\mathbf{CV(r_2)} = \langle 3, 6, 44\rangle$; these are inputs to e-MRCM. Fig. 14 illustrates the process of e-MRCM. First, e-MRCM initializes four data structures, namely GT_1, GT_2, FT, and SL. The target concentrations are initialized as two

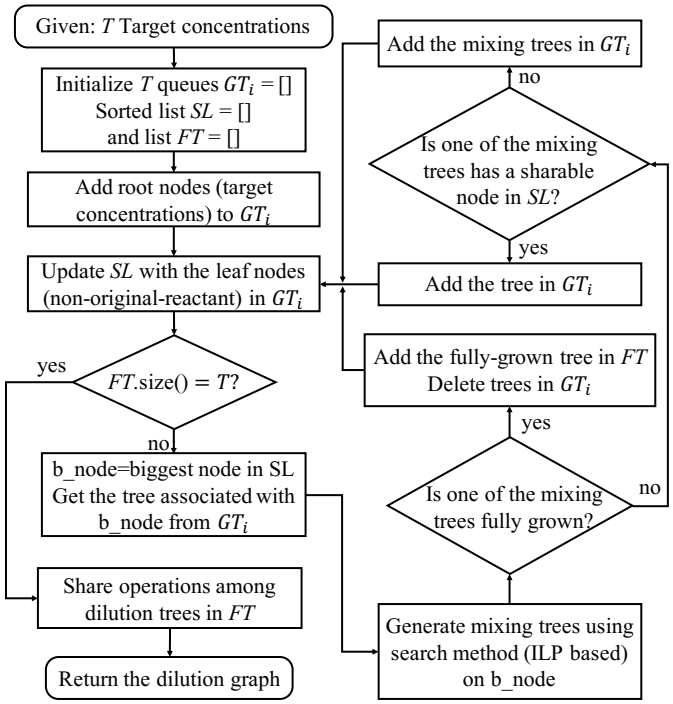

Fig. 12: The overall procedural flow of e-MRCM.

Input: T target concentrations ($\mathbf{CV_1}$ to $\mathbf{CV_T}$)
Output: A list of fully-grown trees FT

```
for i in range(0, T) do
    GT_i = [node(CV_i)];
SL = []; FT = [];
for i in range(0, T) do
    Add leave nodes in GT_i to SL;
while FT.size() != T do
    b_node = biggest node in SL;
    GT_j = the tree that contains b_node;
    Trees = all possible mixing trees obtained from ILP-search(b_node);
    if One tree in Trees is fully grown then
        Add this tree in FT; GT_j = [];
    else
        if One tree in Trees has sharable node in SL then
            Add this tree in GT_j; Update all GT_i;
        else
            Add Trees in GT_j;
    for i in range(0, T) do
        Update leave nodes in GT_i to SL;
Share common operations in FT;
return FT
```

Fig. 13: Pseudocode for e-MRCM.

nodes and stored in GT_1 and GT_2, respectively; see Fig. 14(a). Leave nodes in GT_1 and GT_2 are also stored in the priority queue SL. As shown in Fig. 14(b), e-MRCM then explores possible mixing opportunities for the first node in SL, which is $\mathbf{CV(r_1)}$, and adds the partially-grown trees back to GT_1. After the trees are added back to GT_1, leave nodes are updated in SL. Next, as shown in Fig. 14(c), e-MRCM explores possible mixing opportunities for the first node in SL, which is

This article has been accepted for publication in a future issue of this journal, but has not been fully edited. Content may change prior to final publication. Citation information: DOI 10.1109/TCAD.2019.2942002, IEEE Transactions on Computer-Aided Design of Integrated Circuits and Systems

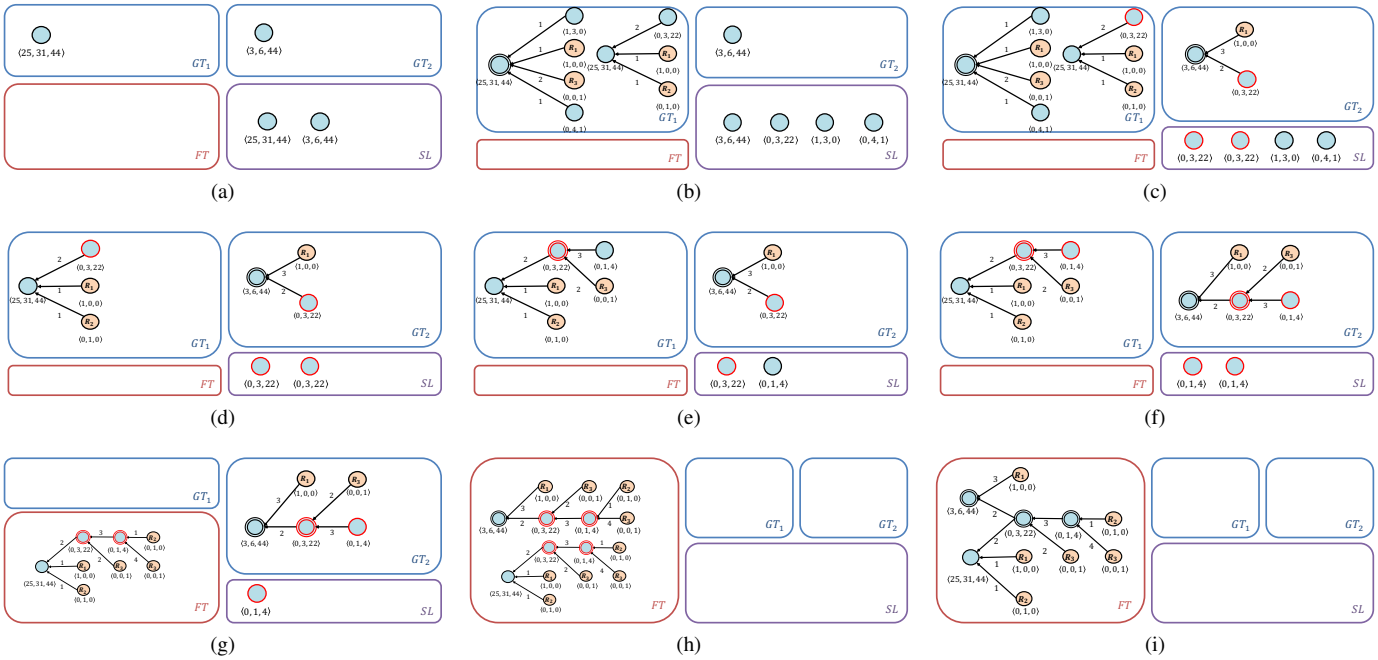

Fig. 14: An example of generating sharable dilution processes of two target concentrations, $\mathbf{CV}(\mathbf{r_1}) = \langle 25, 31, 44 \rangle$ and $\mathbf{CV}(\mathbf{r_2}) = \langle 3, 6, 44 \rangle$, using e-MRCM. The dilution-graph-generation process is detailed in Section V.

$\mathbf{CV}(\mathbf{r_2})$, and adds the partially-grown tree back to GT_2. When the nodes are updated in SL, e-MRCM identifies the sharable nodes of distinct trees in GT_1 and GT_2. Therefore, as shown in Fig. 14(d), e-MRCM keeps the sharable tree in GT_1 and discards the other tree. Afterwards, e-MRCM explores mixing opportunities on the first node in SL for several iterations (Fig. 14(e) to Fig. 14(f)) until a fully-grown tree is produced. The fully-grown trees are added to FT; see Fig. 14(g) and Fig. 14(h). Finally, the iteration of exploring mixing opportunities stops because two dilution trees have been produced for the two target concentrations. As shown in Fig. 14(i), common operation in dilution trees are shared, and e-MRCM returns the final dilution graph.

VI. Simulation Results

To evaluate the effectiveness of MRCM, we compare it with four existing sample-preparation methods, i.e., BS [10], REMIA [11], CoDOS [16], and WSPM [34]. While BS, REMIA, and CoDOS were developed for sample preparation on traditional DMFBs, WSPM has been designed for MEDA biochips. To compare these methods properly, we consider that the volumes of the target droplet are the same across a DMFB and a MEDA biochip in our experiments. We assume that the gaps between the top plate and the bottom plate are the same. Therefore, the target droplet spans an electrode area of 1×1 (mm^2) on both of the biochips. We assume the electrode size of the DMFB is 1×1 (mm^2) [41]. We conservatively assume that the minimum aliquot droplet spans an area of 0.25×0.25 (mm^2) on a MEDA biochip, i.e., the target droplet is four times as big as the aliquot droplet.

Experiments with different numbers of reactants N are carried out for all the methods, i.e., $2 \leq N \leq 5$. In order to show the effectiveness of the proposed method, we adopt the precision level $P = 1/512$ because precision levels for traditional DMFBs can only be powers of 2. When $N = 2$, all concentration values are considered from $1/512$ to $511/512$; in other experiments, 512 concentrations are randomly generated. All simulations are performed in Python on a workstation with 2.5 GHz Xeon processor and 2 GB memory. We show and discuss the single-target and multiple-target experiments in the next two subsections, respectively.

A. Single-Target Sample Preparation

We first examine the simulation results when $N = 2$, i.e., two reactants are diluted to generate the target concentration. This is usually referred to as sample/reagent and buffer dilution. Samples and reagents are more expensive than the buffer. The precious sample/reagent is diluted with the buffer serially to the target concentration. Therefore, we set the cost of the sample/reagent to be 1 and the cost of the buffer to be 0. The simulation results are presented in Fig. 15. MRCM outperforms WSPM, which is the most efficient sample preparation method on MEDA biochips thus far, in all aspects. Note that MRCM greatly reduces the waste production in comparison with other methods, even though it chooses the best dilution tree primarily based on the minimum reagent consumption.

We then examine the simulation results when $N > 2$. Since REMIA and WSPM were developed only for two-reactant sample preparation, we exclude them in these experiments. Recall that the reactant cost varies from one reagent to another in multiple-reactant sample preparation due to different scenarios. To evaluate the effectiveness of reactant cost minimization in MRCM, we set the costs of reactants in a geometric sequence from 1 to 64, which is the same setup as in the previous method [16]. The simulation results are presented in Table II. When $N = 3$, MRCM reduces the number of operations by 37% and 19% in comparison with BS and

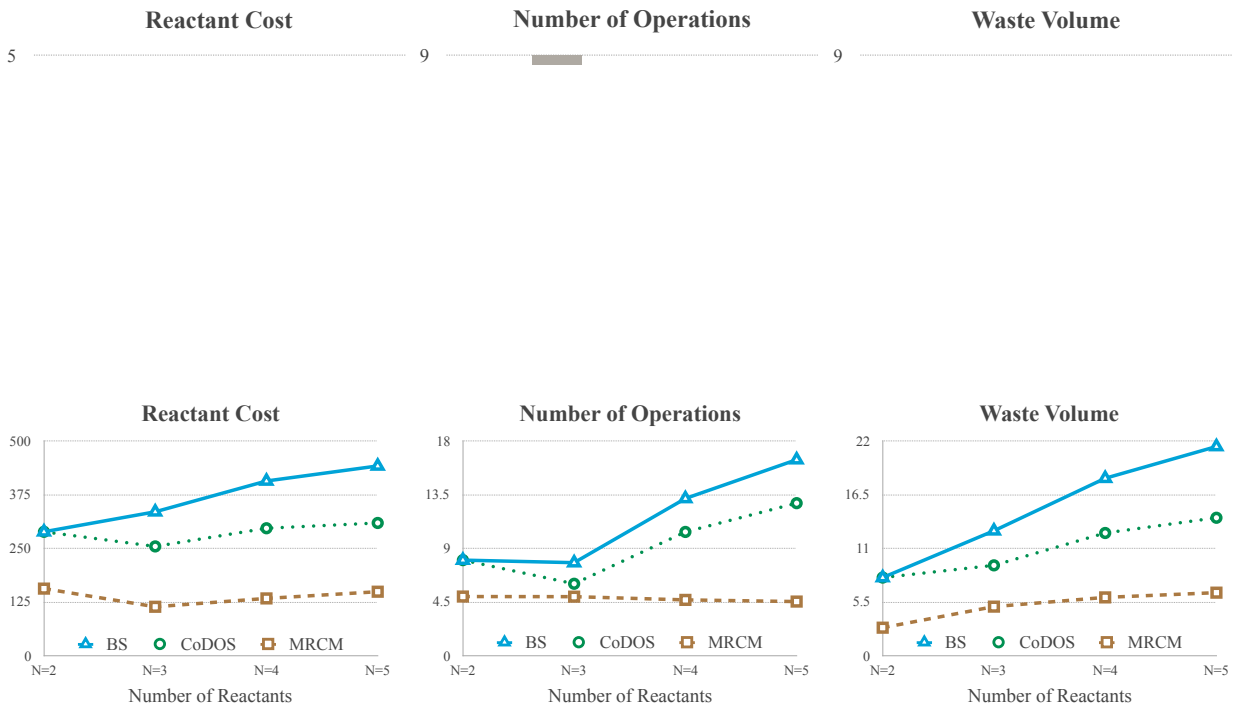

Fig. 16: Comparison between BS, CoDOS, and MRCM for multiple-reactant sample preparation.

TABLE II: Results of Multiple-Reactant Sample Preparation.

$N = 3$	Reactant Usage	Number of Operations	Waste Volume	Reactant Cost
BS	13.82 (45%)[a]	7.82 (63%)	12.82 (33%)	335.45 (34%)
CoDOS	10.28 (60%)	6.05 (81%)	9.28 (46%)	254.94 (45%)
MRCM	6.18	4.93	4.23	114.56
$N = 4$	**Reactant Usage**	**Number of Operations**	**Waste Volume**	**Reactant Cost**
BS	19.19 (39%)	13.19 (35%)	18.19 (30%)	407.11 (33%)
CoDOS	13.59 (54%)	10.39 (44%)	12.59 (43%)	297.19 (45%)
MRCM	7.93	4.6	5.39	133.98
$N = 5$	**Reactant Usage**	**Number of Operations**	**Waste Volume**	**Reactant Cost**
BS	22.44 (37%)	16.44 (27%)	21.44 (30%)	442.08 (34%)
CoDOS	15.15 (54%)	12.80 (36%)	14.15 (46%)	309.46 (48%)
MRCM	8.25	4.38	6.27	149.59

[a]Numbers in parentheses are the ratios between MRCM and the specified method

CoDOS, respectively[1]. As the number of reactants increases to 5, the reduction in the number of operations further improves to 73% and 64%, respectively. In addition, MRCM incurs less reactant costs and produces less fluidic waste than BS and CoDOS from $N = 3$ to $N = 5$. When the cost of each reactant is not considered and $N = 3$, MRCM achieves a reduction in reactant usage by 55% and 40% compared to BS and CoDOS, respectively; after considering the cost of each reactant, the overall cost is further decreased to 66% and 55%. These results highlight the effectiveness of MRCM in reducing the cost associated with the use of expensive reactants.

The results also show that the performance of MRCM is not significantly affected when the number of reactants increases (see Fig. 16). For BS and CoDOS, which are carried out on traditional DMFBs using the (1:1) mixing model, the reactant cost, the number of operations, and the fluidic waste all increase when the number of reactants increases. In contrast, the reactant cost and the fluidic waste increase insignificantly for MRCM. Furthermore, the average number of operations is stable and remains at around 4.8 as the number of reactants increases. The results show that MRCM is a better solution for multiple-reactant sample preparation.

[1]The mixing time for different mixing models may not be the same.

B. Multiple-Target Sample Preparation

In this section, we consider sample preparation scenarios when the number of reactants ranges from 2 to 5. For each choice of the number of reactants, we conducted experiments by varying the number of target concentrations from 2 to 5. A total of 50 concentration sets are randomly generated for each pair of the number of reactants and the number of targets; the averaged results of these experiments are summarized in Table III. To be consistent with the experiments in the previous subsection, we also set the costs of reactants in a geometric sequence from 1 to 64. Similar to the results in the previous subsection, MRCM also performs better in terms of the reactant cost, the number of operations, and waste production for multiple-target sample preparation. Even though MRCM outperforms all other previous methods, e-MRCM can achieve even better performance in all aspects. For the two-reactant sample preparation in the five-target-concentrations experiment, e-MRCM further reduces the reactant cost, the number of operations, and the waste production by 8.06%, 9.09%, and 15.15%, respectively. The results show that e-MRCM can find sharing opportunities between dilution trees using a heuristic approach, and the performance of e-MRCM is better than that of MRCM for multiple-target sample preparation.

VII. Conclusion

We have discussed the comparison between sample preparation methods on conventional DMFBs and that on MEDA biochips. We have also described unique MEDA-enable operations, and exploited these operations to optimize sample preparation using a general mixing model. Based on this

TABLE III: Results of Multiple-target Sample Preparation.

N = 2	Reactant Cost				Number of Operations				Waste Volume			
# of Targets	BS	CoDOS	MRCM	e-MRCM	BS	CoDOS	MRCM	e-MRCM	BS	CoDOS	MRCM	e-MRCM
2	678.66	678.66	334.14	327.45	16.42	16.42	10.78	10.52	16.42	16.42	6.32	5.93
3	960.42	960.42	489.60	469.04	23.76	23.76	16.76	15.98	23.76	23.76	9.21	8.18
4	1,325.78	1,325.78	660.35	608.57	32.80	32.80	22.06	20.14	32.80	32.80	12.90	10.26
5	1,652.56	1,652.56	829.63	762.74	41.06	41.06	27.28	24.80	41.06	41.06	16.38	12.26
N = 3	Reactant Cost				Number of Operations				Waste Volume			
# of Targets	BS	CoDOS	MRCM	e-MRCM	BS	CoDOS	MRCM	e-MRCM	BS	CoDOS	MRCM	e-MRCM
2	550.70	486.62	224.44	222.69	14.76	12.40	9.94	9.82	20.76	16.04	10.02	9.81
3	814.24	718.64	343.03	335.91	23.28	19.30	14.92	14.52	32.28	24.32	15.10	14.49
4	1,105.18	957.54	460.78	445.31	29.94	24.58	19.88	19.26	41.94	31.22	19.83	18.64
5	1,371.08	1,203.46	569.62	551.95	37.32	30.72	24.80	23.82	52.32	39.12	25.10	23.32
N = 4	Reactant Cost				Number of Operations				Waste Volume			
# of Targets	BS	CoDOS	MRCM	e-MRCM	BS	CoDOS	MRCM	e-MRCM	BS	CoDOS	MRCM	e-MRCM
2	765.28	524.44	256.66	253.53	28.76	22.46	9.52	9.42	34.76	22.16	11.88	11.78
3	1,185.56	811.04	395.63	394.69	43.58	34.10	13.96	13.90	52.58	33.62	17.99	17.92
4	1,579.60	1,115.32	533.39	528.69	58.56	45.96	18.76	18.56	70.56	45.36	23.97	23.74
5	1,970.36	1,359.80	650.26	643.36	73.50	57.36	23.86	23.54	88.50	56.22	29.34	28.95
N = 5	Reactant Cost				Number of Operations				Waste Volume			
# of Targets	BS	CoDOS	MRCM	e-MRCM	BS	CoDOS	MRCM	e-MRCM	BS	CoDOS	MRCM	e-MRCM
2	804.55	620.05	297.17	297.17	31.98	25.54	9.16	9.16	37.98	25.10	13.04	13.04
3	1,205.37	939.91	442.40	441.63	48.80	39.14	13.68	13.62	57.80	38.48	19.29	19.18
4	1,621.42	1,229.49	597.50	596.85	66.62	52.86	18.38	18.36	78.62	51.10	25.95	25.93
5	2,061.21	1,556.80	756.94	750.86	83.48	66.32	22.84	22.60	98.48	64.16	32.94	32.64

mixing model, we have proposed the first multiple-reactant sample preparation algorithm, named MRCM, on MEDA biochips. In order to enhance MRCM for multiple-target sample preparation, we have also presented e-MRCM, and e-MRCM generates dilution trees with the better sharing opportunities. The simulated experiments have shown the effectiveness of the proposed algorithm in terms of the number of operations, reactant cost, and waste volume.

REFERENCES

[1] T.-C. Liang, Y.-S. Chan, T.-Y. Ho, K. Chakrabarty, and C.-Y. Lee, "Sample preparation for multiple-reactant bioassays on micro-electrode-dot-array biochips," in *Proc. ACM Asia and South Pacific Design Automation Conference (ASP-DAC)*, 2019, pp. 468–473.

[2] J. M. Andrews, "Determination of minimum inhibitory concentrations," *Journal of antimicrobial Chemotherapy*, vol. 48, no. suppl_1, pp. 5–16, 2001.

[3] S. Bhattacharjee, A. Banerjee, T.-Y. Ho, K. Chakrabarty, and B. B. Bhattacharya, "Efficient generation of dilution gradients with digital microfluidic biochips," *IEEE Transactions on Computer-Aided Design of Integrated Circuits and Systems (TCAD)*, 2018.

[4] P. R. Gascoyne and J. V. Vykoukal, "Dielectrophoresis-based sample handling in general-purpose programmable diagnostic instruments," *Proceedings of the IEEE*, vol. 92, no. 1, pp. 22–42, 2004.

[5] H. Kim, M. S. Bartsch, R. F. Renzi, J. He, J. L. Van de Vreugde, M. R. Claudnic, and K. D. Patel, "Automated digital microfluidic sample preparation for next-generation DNA sequencing," *Journal of the Association for Laboratory Automation*, vol. 16, no. 6, pp. 405–414, 2011.

[6] R. Sista, Z. Hua, P. Thwar, A. Sudarsan, V. Srinivasan, A. Eckhardt, M. Pollack, and V. Pamula, "Development of a digital microfluidic platform for point of care testing," *Lab on a Chip*, vol. 8, no. 12, pp. 2091–2104, 2008.

[7] L. Malic, T. Veres, and M. Tabrizian, "Biochip functionalization using electrowetting-on-dielectric digital microfluidics for surface plasmon resonance imaging detection of DNA hybridization," *Biosensors and Bioelectronics*, vol. 24, no. 7, pp. 2218–2224, 2009.

[8] P. Paik, V. K. Pamula, and R. B. Fair, "Rapid droplet mixers for digital microfluidic systems," *Lab on a Chip*, vol. 3, no. 4, pp. 253–259, 2003.

[9] S. K. Cho, H. Moon, and C.-J. Kim, "Creating, transporting, cutting, and merging liquid droplets by electrowetting-based actuation for digital microfluidic circuits," *Journal of Microelectromechanical systems*, vol. 12, no. 1, pp. 70–80, 2003.

[10] W. Thies, J. P. Urbanski, T. Thorsen, and S. Amarasinghe, "Abstraction layers for scalable microfluidic biocomputing," *Natural Computing*, vol. 7, no. 2, pp. 255–275, 2008.

[11] J.-D. Huang, C.-H. Liu, and T.-W. Chiang, "Reactant minimization during sample preparation on digital microfluidic biochips using skewed mixing trees," in *Proc. IEEE/ACM International Conference on Computer-Aided Design (ICCAD)*, 2012, pp. 377–383.

[12] H. Wang, M. Qi, and A. J. Cutler, "A simple method of preparing plant samples for PCR." *Nucleic Acids Research*, vol. 21, no. 17, p. 4153, 1993.

[13] P. S. Dittrich and A. Manz, "Lab-on-a-chip: microfluidics in drug discovery," *Nature Reviews Drug Discovery*, vol. 5, no. 3, p. 210, 2006.

[14] C. Kleinstreuer, J. Li, and J. Koo, "Microfluidics of nano-drug delivery," *International Journal of Heat and Mass Transfer*, vol. 51, no. 23-24, pp. 5590–5597, 2008.

[15] R. Bonfiglio, R. C. King, T. V. Olah, and K. Merkle, "The effects of sample preparation methods on the variability of the electrospray ionization response for model drug compounds," *Rapid Communications in Mass Spectrometry*, vol. 13, no. 12, pp. 1175–1185, 1999.

[16] C.-H. Liu, H.-H. Chang, T.-C. Liang, and J.-D. Huang, "Sample preparation for many-reactant bioassay on dmfbs using common dilution operation sharing," in *Proc. IEEE/ACM International Conference on Computer-Aided Design (ICCAD)*, 2013, pp. 615–621.

[17] S. Kumar, S. Roy, P. P. Chakrabarti, B. B. Bhattacharya, and K. Chakrabarty, "Efficient mixture preparation on digital microfluidic biochips," in *Proc. IEEE International Symposium on Design and Diagnostics of Electronic Circuits & Systems (DDECS)*, 2013, pp. 205–210.

[18] S. Roy, S. Kumar, P. P. Chakrabarti, B. B. Bhattacharya, and K. Chakrabarty, "Demand-driven mixture preparation and droplet streaming ing digital microfluidic biochips," in *Proc. ACM Design Automation Conference (DAC)*, 2014, pp. 1–6.

[19] S. Roy, P. P. Chakrabarti, S. Kumar, K. Chakrabarty, and B. B. Bhattacharya, "Layout-aware mixture preparation of biochemical fluids on application-specific digital microfluidic biochips," *ACM Transactions on Design Automation of Electronic Systems (TODAES)*, vol. 20, no. 3, p. 45, 2015.

[20] O. Henegariu, N. Heerema, S. Dlouhy, G. Vance, and P. Vogt, "Multiplex PCR: critical parameters and step-by-step protocol," *Biotechniques*, vol. 23, no. 3, pp. 504–511, 1997.

[21] I. M. Mackay, K. E. Arden, and A. Nitsche, "Real-time PCR in virology," *Nucleic Acids Research*, vol. 30, no. 6, pp. 1292–1305, 2002.

[22] W. Rychlik, W. Spencer, and R. Rhoads, "Optimization of the annealing temperature for DNA amplification in vitro," *Nucleic Acids Research*, vol. 18, no. 21, pp. 6409–6412, 1990.

[23] K. H. Roux, "Optimization and troubleshooting in PCR," *Genome Research*, vol. 4, no. 5, pp. S185–S194, 1995.

[24] H. A. Erlich *et al.*, *PCR Technology*. Springer, 1989.

[25] M. Gustafsson, D. Hirschberg, C. Palmberg, H. Jörnvall, and T. Bergman, "Integrated sample preparation and maldi mass spectrometry on a microfluidic compact disk," *Analytical Chemistry*, vol. 76, no. 2, pp. 345–350, 2004.

[26] A. R. Wheeler, H. Moon, C. A. Bird, R. R. Ogorzalek Loo, C.-J. . Kim, J. A. Loo, and R. L. Garrell, "Digital microfluidics with in-line sample purification for proteomics analyses with maldi-ms," *Analytical Chemistry*, vol. 77, no. 2, pp. 534–540, 2005.

[27] D. T. Wang, Gary and S.-K. Fan, "Digital microfluidic operations on micro-electrode dot array architecture," *IET Nanobiotechnology*, vol. 5, no. 4, pp. 152–160, 2011.

[28] K. Y.-T. Lai, Y.-T. Yang, and C.-Y. Lee, "An intelligent digital microfluidic processor for biomedical detection," *Journal of Signal Processing Systems*, vol. 78, no. 1, pp. 85–93, 2015.

[29] T.-C. Liang, M. Shayan, K. Chakrabarty, and R. Karri, "Execution of provably secure assays on MEDA biochips to thwart attacks," in *Proc. ACM Asia and South Pacific Design Automation Conference (ASP-DAC)*, 2019, pp. 51–57.

[30] C.-M. Huang, C.-H. Liu, and J.-D. Huang, "Volume-oriented sample preparation for reactant minimization on flow-based microfluidic biochips with multi-segment mixers," in *Proc. IEEE Design, Automation & Test in Europe Conference & Exhibition (DATE)*, 2015, pp. 1114–1119.

[31] S. Bhattacharjee, S. Poddar, S. Roy, J.-D. Huang, and B. B. Bhattacharya, "Dilution and mixing algorithms for flow-based microfluidic biochips," *IEEE Transactions on Computer-Aided Design of Integrated Circuits and Systems (TCAD)*, vol. 36, no. 4, pp. 614–627, 2016.

[32] Z. Li, K. Y.-T. Lai, K. Chakrabarty, T.-Y. Ho, and C.-Y. Lee, "Sample preparation on micro-electrode-dot-array digital microfluidic biochips," in *Proc. IEEE Computer Society Annual Symposium on VLSI (ISVLSI)*, 2017, pp. 146–151.

[33] S. Saha, D. Kundu, S. Roy, S. Bhattacharjee, K. Chakrabarty, P. P. Chakrabarti, and B. B. Bhattacharya, "Factorization based dilution of biochemical fluids with micro-electrode-dot-array biochips," in *Proc. ACM Asia and South Pacific Design Automation Conference (ASP-DAC)*, 2019, pp. 462–467.

[34] Z. Li, K. Y.-T. Lai, K. Chakrabarty, T.-Y. Ho, and C.-Y. Lee, "Droplet size-aware and error-correcting sample preparation using micro-electrode-dot-array digital microfluidic biochips," *IEEE Transactions on Biomedical Circuits And Systems (TBioCAS)*, vol. 11, no. 6, pp. 1380–1391, 2017.

[35] Y. Ho, G. Wang, K. Y.-T. Lai, Y.-W. Lu, K.-M. Liu, Y.-M. Wang, and C.-Y. Lee, "Design of a micro-electrode cell for programmable lab-on-CMOS platform," in *Proc. IEEE International Symposium on Circuits and Systems (ISCAS)*, 2016, pp. 2871–2874.

[36] Z. Li, K. Y.-T. Lai, P.-H. Yu, K. Chakrabarty, T.-Y. Ho, and C.-Y. Lee, "Droplet size-aware high-level synthesis for micro-electrode-dot-array digital microfluidic biochips," *IEEE Transactions on Biomedical Circuits And Systems (TBioCAS)*, vol. 11, no. 3, pp. 612–626, 2017.

[37] Z. Li, K. Y.-T. Lai, J. McCrone, P.-H. Yu, K. Chakrabarty, M. Pajic, T.-Y. Ho, and C.-Y. Lee, "Efficient and adaptive error recovery in a micro-electrode-dot-array digital microfluidic biochip," *IEEE Transactions on Computer-Aided Design of Integrated Circuits and Systems (TCAD)*, vol. 37, no. 3, pp. 601–614, 2018.

[38] Z. Zhong, Z. Li, and K. Chakrabarty, "Adaptive error recovery in micro-electrode-dot-array biochips based on droplet-aliquot operations and predictive analysis," in *Proc. IEEE/ACM International Conference on Computer-Aided Design (ICCAD)*, 2017, pp. 615–622.

[39] Z. Zhong, Z. Li, and K. Chakrabarty, "Adaptive and roll-forward error recovery in meda biochips based on droplet-aliquot operations and predictive analysis," *IEEE Transactions on Multi-Scale Computing Systems (TMSCS)*, vol. 4, no. 4, pp. 577–592, 2018.

[40] G. E. Andrews and K. Eriksson, *Integer Partitions*. Cambridge University Press, 2004.

[41] H. Moon and J. Nikapitiya, "Digital microfluidic devices and methods of dispensing and splitting droplets in digital microfluidic devices," Jun. 23 2016, US Patent App. 14/976,019.

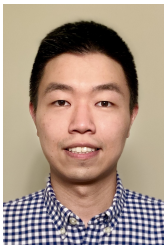

Tung-Che Liang received his B.S. degree in Electronics Engineering from National Chiao Tung University, Hsinchu, Taiwan, in 2014. He is currently working toward the Ph.D. degree with Duke University, Durham, NC, USA.

He was with Synopsys Inc., Hsinchu, Taiwan, as an R&D engineer. He was a yield & diagnosis intern at Intel, Santa Clara, CA, and a DFT intern at NVIDIA Inc., Santa Clara, CA. His current research interests include design automation and security for microfluidic systems.

Yun-Sheng Chan received the B.S. degree from National Dong Hwa University (NDHU) and the M.S. degree from National Chiao Tung University, Hsinchu (NCTU), Taiwan, in 2015 and 2016, respectively, all in electronics engineering. Currently, he is working toward the Ph.D. degree at the Institute of Electronics, National Chiao Tung University, Hsinchu, Taiwan. His research interests focus on digital system design and circuit design for biomedical applications.

Tsung-Yi Ho (SM'10) received his Ph.D. in Electrical Engineering from National Taiwan University in 2005.

He is a Professor with the Department of Computer Science of National Tsing Hua University, Hsinchu, Taiwan. His research interests include design automation and test for microfluidic biochips and neuromorphic computing systems.

He has been the recipient of the Invitational Fellowship of the Japan Society for the Promotion of Science (JSPS), the Humboldt Research Fellowship by the Alexander von Humboldt Foundation, the Hans Fischer Fellowship by the Institute of Advanced Study of the Technische Universitt Mnchen, and the International Visiting Research Scholarship by the Peter Wall Institute of Advanced Study of the University of British Columbia. He was a recipient of the Best Paper Awards at the VLSI Test Symposium in 2013 and IEEE Transactions on Computer-Aided Design of Integrated Circuits and Systems in 2015. Currently, he serves as the principal investigator of the AI Research Program of Ministry of Science and Technology in Taiwan, an ACM Distinguished Speaker, and Associate Editor of the ACM Journal on Emerging Technologies in Computing Systems, ACM Transactions on Design Automation of Electronic Systems, ACM Transactions on Embedded Computing Systems, and IEEE Transactions on Very Large Scale Integration Systems.

Krishnendu Chakrabarty (F'08) received the B.Tech. degree from the Indian Institute of Technology Kharagpur, Kharagpur, India, in 1990 and the M.S.E. and Ph.D. degrees from the University of Michigan, Ann Arbor, MI, USA, in 1992 and 1995, respectively.

He is currently the John Cocke Distinguished Professor and the Department Chair of Electrical and Computer Engineering at Duke University, Durham, NC, USA. His current research interests include testing and design-for-test of system-on-a-chip (SOC) integrated circuits, boards, and systems; microfluidic biochips; hardware security; and neuromorphic computing systems.

Dr. Chakrabarty is a fellow of ACM and AAAS. He was a recipient of the National Science Foundation CAREER Award, the Office of Naval Research Young Investigator Award, the Humboldt Research Award from the Alexander von Humboldt Foundation, Germany, the ACM Transactions on Design Automation of Electronic Systems Best Paper Award in 2016, the IEEE Transactions on CAD Donald O. Pederson Best Paper Award in 2015, over a dozen best paper awards at major conferences, the IEEE Computer Society Technical Achievement Award in 2015, the IEEE Circuits and Systems Society Charles A. Desoer Technical Achievement Award in 2017, and the Semiconductor Research Corporation Technical Excellence Award in 2018.

Chen-Yi Lee received the B.S. degree in electrical engineering from National Chiao Tung University (NCTU), Hsinchu, Taiwan, in 1982 and the M.S. and Ph.D. degrees in electrical engineering from Katholieke University Leuven, Leuven, Belgium, in 1986 and 1990, respectively.

From 1986 to 1990, he was with IMEC/VSDM, Leuven, researching in the area of architecture synthesis for DSP. In 1991, he joined the Department of Electronics Engineering and from 2003 to 2006, he was the Chairman. From 2000 to 2003, he was the Director of National CHIP Implementation Center and the Co-Ordinator of Microelectronics Program of Engineering Division, National Security Council, Taipei, Taiwan. He was the Dean of office of research and development from 2007 to 2010, NCTU. He currently serves as the Co-Program Director of National Program of Intelligent Electronics and a Professor of the Department of Electronics Engineering, NCTU. His current research interests include very large scale integration (VLSI) algorithms and architectures for high-throughput DSP applications. He is also active in various aspects of micro sensing, low-power system-on-chip, and deep learning.

Dr. Lee was a recipient of the Outstanding Technology Licensing Award from National Science Council in 2007 and 2008, the Industry Contribution Award from Ministry of Economic Affairs, and the Outstanding Research Award from National Science Council in 2009. He served as the Program Committee Member of IEEE International Solid-State Circuits Conference in 2004-2006, Design, Automation & Test in Europe Conference TPC Member in 2006 and 2007, IEEE Asian Solid-State Circuits Conference TPC Member in 2006-2014, IEEE VLSI Symposium Committee Member in 2010-2014, IEEE Transactions on Circuits and Systems-II Associate Editor in 2010 and 2011, and the Past-Chair of Taipei Chapter of IEEE Circuits and Systems Society.